Enhanced nonlinear optics in coupled optical microcavities with an unbroken and broken parity-time symmetry

Jiahua Li,[1,2,*] Xiaogui Zhan,[3] Chunling Ding,[4] Duo Zhang,[5] and Ying Wu[1,†]

[1]*School of Physics, Huazhong University of Science and Technology, Wuhan 430074, People's Republic of China*

[2]*Key Laboratory of Fundamental Physical Quantities Measurement of Ministry of Education, Wuhan 430074, People's Republic of China*

[3]*School of Mathematics and Physics, University of South China, Hengyang 421001, People's Republic of China*

[4]*School of Physics and Electronics, Henan University, Kaifeng 475004, People's Republic of China*

[5]*School of Electrical and Electronic Engineering, Wuhan Polytechnic University, Wuhan 430023, People's Republic of China*

(Received 4 August 2015; revised manuscript received 13 September 2015; published 21 October 2015)

We present a perturbation technique to study the linear and nonlinear output characteristics of coherent photon transport in a parity-time ($\mathcal{PT}$)-symmetric double-microcavity system where one passive cavity contains a single quantum emitter. It is found that (i) for the linear transmission of a low-power input probe field, the output spectra of the proposed $\mathcal{PT}$-symmetric system exhibit a single transparent resonance dip and two symmetric, strongly amplifying sidebands, i.e., an inverted dipole-induced transparency; and (ii) for the nonlinear transmission of the input probe field, giant optical third-order nonlinearities with high linear transmission rate and vanishing nonlinear absorption can be achieved efficiently when the system parameters are tuned properly so that a $\mathcal{PT}$-symmetry phase transition occurs. The obtained results can be useful for quantum information processing, quantum nondemolition measurements of photons, and optical signal processing.

DOI: 10.1103/PhysRevA.92.043830 PACS number(s): 42.50.Pq, 11.30.Er, 42.65.Hw, 42.50.Gy

I. INTRODUCTION

In recent years, a special class of physical systems with a so-called parity-time ($\mathcal{PT}$) symmetry has attracted considerable interest due to its potential applications [1–4]. The notions of $\mathcal{PT}$ symmetry are originally proposed within the framework of quantum mechanics as an alternative criterion for a non-Hermitian Hamiltonian that possesses a real eigenvalue spectrum [1,2]. Up to now, the $\mathcal{PT}$ symmetry has been realized experimentally in a variety of physical systems [5–18]. Due to the equivalence between the mathematical frameworks of quantum mechanics and optics, more recently, the photonic system (e.g., two coupled cavities [10,14–16]) has become an excellent platform for exploring the fundamentals of $\mathcal{PT}$ symmetry and tailoring the light-matter interactions, with non-Hermiticity denoted by optical gain and loss [10–18]. For the ideal $\mathcal{PT}$-symmetric setting, the necessary condition requires the balanced gain and loss so that the eigenvalues end up on the real axis. These $\mathcal{PT}$-symmetric systems can exhibit some interesting, counterintuitive properties, especially at a type of exceptional point (EP) in parameter space, where pairs of eigenvalues collide and become complex [3,4]. Specifically, below the EP, $\mathcal{PT}$-symmetric Hamiltonians can be characterized by a real eigenvalue spectrum in spite of the fact that they are non-Hermitian. This condition corresponds to an unbroken $\mathcal{PT}$ symmetry. On the contrary, above the EP, the spectrum ceases to be real and starts to become complex. This condition corresponds to a spontaneously broken $\mathcal{PT}$ symmetry. A phase transition from the unbroken-$\mathcal{PT}$ symmetry to broken-$\mathcal{PT}$ symmetry appears when tuning the parameter in the system Hamiltonian. As a result, the corresponding optical modes can propagate preferentially in one desired spatial location or another, showing either strong gain or loss [19–23]. The $\mathcal{PT}$-symmetric physics that follows from the above-mentioned unique properties has enabled applications ranging from power oscillations violating left-right symmetry [22,23], loss-induced or gain-induced transparency [5,6], unidirectional invisibility [7–9], low-power optical isolation [10–13], efficient photon or phonon lasing [14–17], to ultralow-threshold optical chaos [18], etc.

On the other hand, an optical microcavity coupled to a quantum emitter (QE) is an almost ideal cavity quantum electrodynamics (QED) system for implementing a series of important devices owing to its high-quality factor Q and small mode volume V (see, e.g., the review of Refs. [24–27]). As a natural extension of a single-cavity QED structure, two or more coupled microcavities containing QEs have been widely studied both theoretically and experimentally. However, it should be pointed out that all of these previous investigations were carried out with coupled passive cavities without a $\mathcal{PT}$-symmetric architecture (i.e., lossy cavities, without optical gain). Recently, attention has also focused on the realization and study of $\mathcal{PT}$-symmetric optical systems where one passive cavity is coupled to the other active cavity (i.e., gain cavity) by manipulating the gain-to-loss ratio [10,11,14–16]. It has been shown from these studies that in the $\mathcal{PT}$-symmetric system, introducing optical gain to one of the two cavities can balance the passive loss of the other. For instance, both Peng *et al.* [10] and Chang *et al.* [11], respectively, realized remarkable $\mathcal{PT}$-symmetric behaviors in coupled whispering-gallery-mode (WGM) microresonators by properly adjusting the gain in one active resonator and the loss in the other passive resonator. Moreover, the field localization in the passive resonator and an accompanied enhancement of optical nonlinearity leading to nonreciprocal light transmission are found in such an optical compound structure. Additionally, Peng *et al.* [14], Feng *et al.* [15], and Hodaei *et al.* [16], respectively, reported several types of novel single-mode laser

*huajia_li@163.com
†yingwu2@126.com

behaviors by delicately manipulating the gain-to-loss ratio in the $\mathcal{PT}$-symmetric double cavity.

It is well known that direct interaction between single photons cannot occur according to QED. Optical nonlinearity, for example, via a single QE coupled to a driven cavity, enables the photon-photon interaction. Thus, it is of great importance to achieve high-degree optical nonlinearity at very low mean-photon level, which lies at the heart of several proposals for quantum information processing, quantum nondemolition measurements of photons, optical signal processing [28,29], and other areas. A variety of methods to generate the strong nonlinear effects between photons have been put forward through an optical passive cavity [30–39]. However, here the dependence of light transmission and optical Kerr nonlinearity on the $\mathcal{PT}$ symmetry in a passive-active double-microcavity system via containing a single QE in the passive microcavity is discussed. An important property of the proposed $\mathcal{PT}$-symmetric scheme for generating high transmission rates and giant optical Kerr nonlinearities is very weak driving power. Besides, the optical response for a weak external field works in a low-Q cavity (total Q factor) where the coupling strength between the two-level QE and the cavity is smaller than the cavity decay rate which contains an intrinsic loss rate and an external loss rate. These conditions allow a more practical system parameter range for physical realization, relaxing the requirements of Refs. [37–39]. Physically, the $\mathcal{PT}$-phase transition plays a key role in the field localization-induced dynamical-intensity accumulation, giving rise to the gain dependence of the linear transmission rates and the enhancement of optical Kerr nonlinearities. By following the cavity-scanning technique described in Ref. [40], it also may provide a method to distinguish the $\mathcal{PT}$-symmetric phase and the $\mathcal{PT}$-broken phase via the experimentally detectable linear transmission spectrum or the Kerr-nonlinear coefficient.

This paper is organized as follows: In Sec. II, we describe a physical model, i.e., a compound cavity-QED system with $\mathcal{PT}$ symmetry. Using a perturbation technique, we derive analytical expressions for the linear transmission coefficient and third-order Kerr-nonlinear coefficient of the output field in the weak-excitation approximation. In Sec. III, we discuss linear transmission features by tuning the system parameters and provide the corresponding physical explanation. In Sec. IV, we study in detail optical nonlinearities under the three different configurations (regimes): a passive single cavity (non-$\mathcal{PT}$-symmetric regime), coupled passive-passive double cavity (non-$\mathcal{PT}$-symmetric regime), and coupled passive-active double cavity (unbroken $\mathcal{PT}$-symmetric regime or broken $\mathcal{PT}$-symmetric regime). We also discuss the influences of the QE-cavity detuning and the QE decay rate on optical nonlinearities. Finally, we conclude and give some remarks on our work in Sec. V.

II. THEORETICAL MODEL, EQUATIONS OF MOTION, AND ANALYTICAL SOLUTIONS

As illustrated schematically in Fig. 1, the hybrid system is made up of two directly coupled single-mode cavities via optical tunneling and a two-level QE (atom or atomlike). One of the cavities is passive (i.e., loss), which is represented by bosonic annihilation and creation operators ($\hat{a}_1$, $\hat{a}_1^\dagger$) with

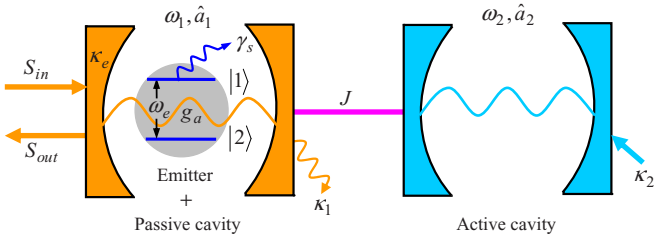

FIG. 1. (Color online) Schematic depiction of a $\mathcal{PT}$-symmetric device including the passive cavity-QED system (with cavity mode $\hat{a}_1$ and QE transitions $\hat{\sigma}_\pm$) coupled to an active cavity $\hat{a}_2$, with a tunneling strength J and a tunable gain-to-loss ratio κ_1, κ_2. The passive cavity mode $\hat{a}_1$, which is driven by an external probe field $S_{\rm in}$ with frequency ω_p and amplitude $\mathcal{E}_p$, is coupled to a QE (gray sphere) with the QE-cavity coupling strength g_a. The QE can be modeled as a two-level quantum system. The gray sphere shows the energy-level structure of the QE. $S_{\rm out}$ is the output of the driving laser field. See text for more details.

resonance frequency ω_1 and cavity decay rate κ_1. The two-level QE (a ground state $|1\rangle$ and an excited state $|2\rangle$) with transition frequency ω_e is placed in the first passive cavity, and the cavity mode $\hat{a}_1$ is coupled to the $|1\rangle \Leftrightarrow |2\rangle$ transition of QE with the coupling strength g_a (also called vacuum Rabi frequency). We refer to this cavity coupled to the QE as the passive cavity-QED system. The second cavity, denoted by bosonic annihilation and creation operators ($\hat{a}_2$, $\hat{a}_2^\dagger$) with resonance frequency $\omega_2 = \omega_1$ and cavity decay rate κ_2, is active (i.e., gain) and is coupled to the first passive cavity owing to the finite overlap of cavity photonic wave functions [10,14–16]. The photon-tunneling (or photon-hopping) strength J between the two cavities can be efficiently modulated by the distance between them. At the same time, an initial single-frequency, continuous-wave (CW) classical input field, which we call the probe field $S_{\rm in}(t) = \mathcal{E}_p e^{-i\omega_p t}$ with the carrier frequency ω_p and the amplitude $\mathcal{E}_p$, is applied to coherently drive the first passive cavity mode. The Hamiltonian of this composite system in the presence of a driving probe field is given by

$$\mathcal{H} = \hbar\omega_e\hat{\sigma}_+\hat{\sigma}_- + \hbar\omega_1\hat{a}_1^\dagger\hat{a}_1 + \hbar\omega_2\hat{a}_2^\dagger\hat{a}_2 + i\hbar g_a(\hat{a}_1\hat{\sigma}_+ - \hat{a}_1^\dagger\hat{\sigma}_-) + \hbar J(\hat{a}_1^\dagger\hat{a}_2 + \hat{a}_2^\dagger\hat{a}_1) + i\hbar\sqrt{\kappa_e}[S_{\rm in}(t)\hat{a}_1^\dagger - S_{\rm in}^*(t)\hat{a}_1], \quad (1)$$

where the rotating-wave approximation (RWA) and the electric-dipole approximation (EDA) have been made. In Eq. (1) above, the first, second, and third terms account for the energy of the uncoupled cavity-QE system. The fourth and fifth terms describe the QE-cavity coupling and the cavity-cavity coupling, respectively. The remaining term represents the driving of the passive cavity by an external laser field. In the derivation of the Hamiltonian, the energy of the QE ground state $|1\rangle$ is set as zero for the sake of simplicity. $\hbar\omega_e$ is the energy of the electronic state $|2\rangle$, that is to say, ω_e is the frequency of the QE's optical transition between the ground state $|1\rangle$ and the excited state $|2\rangle$. The symbol $\hat{\sigma}_- = |1\rangle\langle 2|$ ($\hat{\sigma}_+ = |2\rangle\langle 1| = \hat{\sigma}_-^\dagger$) stands for the descending (ascending) Pauli operator of the QE. On the one hand, the cavity intrinsic loss or gain rate κ_j (loss: $\kappa_j > 0$; gain: $\kappa_j < 0$, $j = 1,2$) is related to the intrinsic quality factor Q_j by $|\kappa_j| = \omega_0/Q_j$. Thus, (i) $\kappa_1 > 0, \kappa_2 > 0$ and (ii) $\kappa_1 > 0, \kappa_2 < 0$

define, respectively, a passive-passive cavity-QED system and a passive-active cavity-QED system. On the other hand, the parameter κ_e is the coupling loss rate between the passive cavity and the taper waveguide, related to the coupling quality factor Q_e by $\kappa_e = \omega_0/Q_e$. Without loss of generality, above we have assumed g_a and J to be real numbers.

Via transforming the above Hamiltonian (1) into the rotating frame at the frequency ω_p of the probe laser field by means of $\mathcal{H}_{\text{free}} = \hbar\omega_p(\hat{\sigma}_+\hat{\sigma}_- + \hat{a}_1^\dagger\hat{a}_1 + \hat{a}_2^\dagger\hat{a}_2)$, $U(t) = e^{-i\mathcal{H}_{\text{free}}t/\hbar} = e^{-i\omega_p t(\hat{\sigma}_+\hat{\sigma}_- + \hat{a}_1^\dagger\hat{a}_1 + \hat{a}_2^\dagger\hat{a}_2)}$, and $\mathcal{H}_{\text{rot}} = U^\dagger(t)\mathcal{H}U(t) - iU^\dagger(t)\frac{\partial U(t)}{\partial t} = U^\dagger(t)(\mathcal{H} - \mathcal{H}_{\text{free}})U(t)$, we can derive the resulting effective Hamiltonian as

$$\begin{aligned}\mathcal{H}_{\text{rot}} &= \hbar(\Delta+\delta)\hat{\sigma}_+\hat{\sigma}_- + \hbar\Delta\hat{a}_1^\dagger\hat{a}_1 + \hbar\Delta\hat{a}_2^\dagger\hat{a}_2 \\ &\quad + i\hbar g_a(\hat{a}_1\hat{\sigma}_+ - \hat{a}_1^\dagger\hat{\sigma}_-) + \hbar J(\hat{a}_1^\dagger\hat{a}_2 + \hat{a}_2^\dagger\hat{a}_1) \\ &\quad + i\hbar\sqrt{\kappa_e}(\mathcal{E}_p\hat{a}_1^\dagger - \mathcal{E}_p^*\hat{a}_1), \end{aligned} \tag{2}$$

where $\Delta = \omega_0 - \omega_p$ (setting $\omega_1 = \omega_2 = \omega_0$) and $\delta = \omega_e - \omega_0$ are, respectively, the detunings of the cavity resonance frequency ω_0 from the probe laser ω_p and the QE transition frequency ω_e from the cavity mode ω_0. In the above, $\mathcal{E}_p$ is the classical amplitude of the monochromatic driving laser field propagating in the output waveguide, which is normalized to a photon flux at the input of the cavity and directly related to the power P_{in} propagating in the output waveguide by the relationship $|\mathcal{E}_p| = \sqrt{\frac{P_{\text{in}}}{\hbar\omega_p}}$.

Our analysis is based on the semiclassical Heisenberg-Langevin equations that are derivable from the Hamiltonian of Eq. (2). Including losses in both the cavity and QE, as well as the cavity excitation, we apply the Heisenberg-Langevin formalism to attain the Heisenberg-Langevin equations of motion (setting the observable $o = \langle\hat{o}\rangle$, where $\hat{o}$ is any operator) together with the standard input-output relation [41,42] as follows:

$$\frac{da_1}{dt} = -(i\Delta + \kappa_1/2 + \kappa_e/2)a_1 - g_a\sigma_- - iJa_2 + \sqrt{\kappa_e}\mathcal{E}_p, \tag{3}$$

$$\frac{da_2}{dt} = -(i\Delta + \kappa_2/2)a_2 - iJa_1, \tag{4}$$

$$\frac{d\sigma_z}{dt} = -\gamma_s(\sigma_z + 1/2) + g_a a_1^*\sigma_- + g_a a_1\sigma_-^*, \tag{5}$$

$$\frac{d\sigma_-}{dt} = -[i(\Delta+\delta) + \gamma_s/2]\sigma_- - 2g_a a_1\sigma_z, \tag{6}$$

$$S_{\text{out}} = S_{\text{in}} - \sqrt{\kappa_e}a_1, \tag{7}$$

with $\sigma_z = (\langle\hat{\sigma}_+\hat{\sigma}_-\rangle - \langle\hat{\sigma}_-\hat{\sigma}_+\rangle)/2$ being the half-population difference between the excited state $|2\rangle$ and the ground state $|1\rangle$. Equations (3) and (4) describe the dynamics of both passive and active cavity modes. Equations (5) and (6) describe the dynamics of the two-level QE. γ_s is the spontaneous decay rate of the two-level QE. Here, the quantum correlations of the photon electron have been safely neglected in the semiclassical approximation, which is valid in the concerned weak-coupling regime, i.e., $g_a < (\kappa_1 + \kappa_e)/2$ and by using a classical low-power driving field [43,44].

Now, we will seek the steady-state solution of Eqs. (3)–(7) in the weak-excitation approximation, where the intensity of the cavity field is small because of the weak-probe driving. In the weak-excitation limit, the perturbation approach can be applied to both the cavity modes and the two-level QE, which is introduced in terms of perturbation expansion as

$$a_1 = \lambda a_1^{(1)} + \lambda^2 a_1^{(2)} + \lambda^3 a_1^{(3)} + \cdots, \tag{8}$$

$$a_2 = \lambda a_2^{(1)} + \lambda^2 a_2^{(2)} + \lambda^3 a_2^{(3)} + \cdots, \tag{9}$$

$$\sigma_z = \sigma_z^{(0)} + \lambda\sigma_z^{(1)} + \lambda^2\sigma_z^{(2)} + \lambda^3\sigma_z^{(3)} + \cdots, \tag{10}$$

$$\sigma_- = \sigma_-^{(0)} + \lambda\sigma_-^{(1)} + \lambda^2\sigma_-^{(2)} + \lambda^3\sigma_-^{(3)} + \cdots, \tag{11}$$

where λ is a continuously varying parameter ranging from zero to unity. Our analysis works in the weak-excitation limit, where the electron in the two-level QE is predominantly populated in the initial ground state $|1\rangle$. In this situation, we directly have the results $\sigma_z^{(0)} = -1/2$ and $\sigma_-^{(0)} = 0$ for the zeroth-order electronic operators. We substitute the above perturbation expansion (8)–(11) into Eqs. (3)–(6) and keep the terms up to the third order in the amplitude of the cavity field. Solving them again can yield the following results for the amplitude of the cavity field a_1:

$$a_1^{(1)} = \frac{\sqrt{\kappa_e}d_1}{g_a^2 + d_1 d_2}\mathcal{E}_p, \tag{12}$$

$$a_1^{(2)} = 0, \tag{13}$$

$$\begin{aligned} a_1^{(3)} &= \frac{2g_a^4}{\gamma_s(g_a^2 + d_1 d_2)}\left(\frac{1}{d_1} + \frac{1}{d_1^*}\right)\frac{\sqrt{\kappa_e}d_1}{g_a^2 + d_1 d_2} \\ &\quad \times \left|\frac{\sqrt{\kappa_e}d_1}{g_a^2 + d_1 d_2}\right|^2 \mathcal{E}_p|\mathcal{E}_p|^2, \end{aligned} \tag{14}$$

where $d_1 = i(\Delta+\delta) + \gamma_s/2$ and $d_2 = i\Delta + \kappa_1/2 + \kappa_e/2 + \Omega$, with $\Omega = \frac{J^2}{i\Delta + \kappa_2/2}$ originating from the coupling of the second cavity. Obviously, the term d_2 is closely dependent on J and κ_2. When $J = 0$, we have the result $\Omega = 0$ and thus the $\mathcal{PT}$-symmetric arrangement reduces to a single passive cavity structure. Since $\mathcal{E}_p$ is the input driving field, all of the nonzero terms in Eqs. (12)–(14) are dependent on $\mathcal{E}_p$.

By using the input-output relation (7), the transmission field S_{out} can be obtained as follows:

$$\begin{aligned} S_{\text{out}} &= \mathcal{E}_p - \sqrt{\kappa_e}a_1^{(1)} - \sqrt{\kappa_e}a_1^{(3)} \\ &= \chi^{(1)}\mathcal{E}_p - \chi^{(3)}|\mathcal{E}_p|^2\mathcal{E}_p, \end{aligned} \tag{15}$$

with the respective coefficients $\chi^{(1)} = 1 - \frac{\kappa_e d_1}{g_a^2 + d_1 d_2}$ and $\chi^{(3)} = \frac{2g_a^4\kappa_e^2}{\gamma_s(g_a^2 + d_1 d_2)}(\frac{1}{d_1} + \frac{1}{d_1^*})\frac{d_1}{g_a^2 + d_1 d_2}|\frac{d_1}{g_a^2 + d_1 d_2}|^2$.

From the above expression (15), it is easy to see that S_{out} is proportional to $\mathcal{E}_p$ and $|\mathcal{E}_p|^2\mathcal{E}_p$, respectively. Therefore, such an expression can correspondingly be an analogy to the linear and third-order nonlinear polarization. The term S_{out} exhibits the linear response and the Kerr-nonlinear response of the coupled QE-cavity compound system to the input probe field. Specifically, $|\chi^{(1)}|^2$ stands for the normalized linear intensity transmission rate of the $\mathcal{PT}$-symmetric system, while the

real part $\mathrm{Re}[\chi^{(3)}]$ corresponds to Kerr nonlinearity and the imaginary part $\mathrm{Im}[\chi^{(3)}]$ corresponds to nonlinear absorption. Note that when $J = 0$, the linear intensity transmission rate $|\chi^{(1)}|^2$ is reduced to some previous results about dipole-induced transparency (DIT) [31,38,45]. From the definition in [40], the Kerr-nonlinear coefficient is given by $n_2 = \frac{\mathrm{Re}[\chi^{(3)}]}{c\varepsilon_0}$, where c is the speed of light in vacuum and ε_0 is the vacuum permittivity. It is easy to find from Eq. (15) that the third-order nonlinear optical effects exist due to the coherent QE-cavity coupling. When $g_a = 0$, we obtain the result $\chi^{(3)} = 0$.

Before proceeding, it should be pointed out that the present coupled cavity-QED system possesses a $\mathcal{PT}$-symmetric phase transition from the $\mathcal{PT}$-symmetric phase to the $\mathcal{PT}$-broken phase when the photon-tunneling strength J/κ_1 (also called photon-tunneling-to-loss ratio) or the gain κ_2/κ_1 (also called gain-to-loss ratio) in the passive-active double cavity is adjusted to pass through the EP, i.e., $J = (\kappa_1 + \kappa_e - \kappa_2)/4$ [10,11]. It is also shown that the threshold of symmetry breaking depends solely on the relation between gain and/or loss and optical tunneling. At the EP, the eigenstates and the corresponding eigenvalues of the $\mathcal{PT}$-symmetric system coalesce. This standard $\mathcal{PT}$-phase transition can significantly influence the dynamics of the cavity-QED system. Diagonalizing the coefficient matrix of both Eqs. (3) and (4) can approximatively obtain the threshold of the above EP under the condition that the small EP shift induced by the QE-cavity interaction is ignored, which is valid in the weak-coupling regime [9,46]. For convenience, we scale the system parameters with respect to the dissipation rate of the first cavity κ_a in the following.

III. LINEAR TRANSMISSION FEATURES: DIT AND INVERTED-DIT PROFILES

In Fig. 2, we plot the normalized linear transmission of the weak-probe input field as a function of the detuning Δ/κ_1 (in units of κ_1) between the cavity mode and the weak-probe field for the three different arrangements: (i) a passive single cavity ($J/\kappa_1 = 0$), (ii) a passive-passive double cavity ($J/\kappa_1 = 3$, $\kappa_2/\kappa_1 = 6$), and (iii) a $\mathcal{PT}$-symmetric (i.e., passive-active) double cavity ($J/\kappa_1 = 3$, $\kappa_2/\kappa_1 = -6$). For the case of a passive single cavity ($J/\kappa_1 = 0$), the transmission spectrum exhibits a conventional DIT profile, quantified by a transparency window and two symmetric sideband dips (see the blue dashed line in Fig. 2) [31,38,45]. Alternatively, a transparency on-resonance peak appears at $\Delta = 0$. This transparency effect is quite analogous to that of the atomic electromagnetically induced transparency (EIT) system [47–50]. For the case of a passive-passive double cavity ($J/\kappa_1 = 3$, $\kappa_2/\kappa_1 = 6$), this system still features a DIT profile except that two sideband dips become deeper and they are shifted towards both sides (see the green dotted line of Fig. 2). For the case of a $\mathcal{PT}$-symmetric double cavity ($J/\kappa_1 = 3$, $\kappa_2/\kappa_1 = -6$), the transmission line shapes transit from a conventional DIT profile to the inverted-DIT profile [6], quantified by a single transparent resonance dip and two symmetric, strongly amplifying sideband peaks (see the red solid line in Fig. 2).

In Fig. 3, we display the normalized linear transmission characteristics of the weak-probe input field by changing the

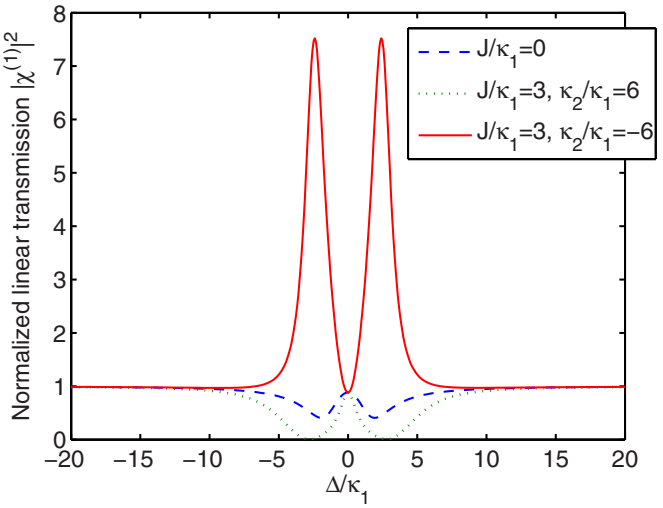

FIG. 2. (Color online) The linear transmission rate $|\chi^{(1)}|^2$ of the probe field as a function of the detuning Δ/κ_1 for three different values of the set $(J/\kappa_1, \kappa_2/\kappa_1)$. Notice that when $J = 0$, corresponding to a single passive cavity structure, we have $\Omega = 0$, which is independent of κ_2. According to recent microcavity experiments [10,11,14], the typical values of system parameters for the numerical results are chosen as $g_a = 2\kappa_1$, $\kappa_e = 5\kappa_1$, $\gamma_s = 0.1\kappa_1$, and $\delta = 0$, respectively.

values of the gain-to-loss ratio κ_2/κ_1 from the loss to the gain in the second cavity, but with a fixed photon-tunneling strength ($J/\kappa_1 = 3$). As can be seen from Fig. 3(a), increasing the loss in the second cavity from $\kappa_2/\kappa_1 = 0$ to $\kappa_2/\kappa_1 = 6$ results in two deeper sidebands and a shallower on-resonance ($\Delta = 0$) transmission peak. When the gain (i.e., $\kappa_2/\kappa_1 < 0$) instead of the loss (i.e., $\kappa_2/\kappa_1 > 0$) is introduced into the second cavity, the transmission behaves as a transition from a conventional DIT profile to an inverted-DIT profile. Increasing the gain in the second cavity from $\kappa_2/\kappa_1 = -2$ to $\kappa_2/\kappa_1 = -6$ helps to increase the heights of the two amplifying sideband peaks. However, as the gain is increased further to a higher value $\kappa_2/\kappa_1 = -10$, both of the sideband peaks are suppressed, as shown in Fig. 3(b). This change is opposite to the observation of monotonically increasing sideband peaks in the atomic EIT system [47–50].

In what follows, we give the physical explanations of the above linear transmission features in Figs. 2 and 3. Under the condition of the fixed photon-tunneling strength $J/\kappa_1 = 3$, the system is in the $\mathcal{PT}$-symmetric phase when $-6 < \kappa_2/\kappa_1 < 0$. However, when $\kappa_2/\kappa_1 < -6$, the system is pushed into the $\mathcal{PT}$-broken phase. So, for the case that $-6 < \kappa_2/\kappa_1 < 0$, the provided gain compensates a portion of the losses, which effectively reduces the loss in the system and hence increases the value of the transmission $|\chi^{(1)}|^2$. Increasing the gain above the EP puts the system in the $\mathcal{PT}$-broken phase, with a localized net loss in the passive cavity, i.e., the field intensity in the passive resonator is significantly decreased [6,10]. Correspondingly, this reduces the strength of the QE-cavity interactions and hence diminishes the value of the transmission $|\chi^{(1)}|^2$. When $\kappa_2/\kappa_1 > 0$, the $\mathcal{PT}$-symmetric system returns to a passive-passive system. In the passive-passive system, the intracavity field localization phenomenon cannot appear, leading to a DIT profile.

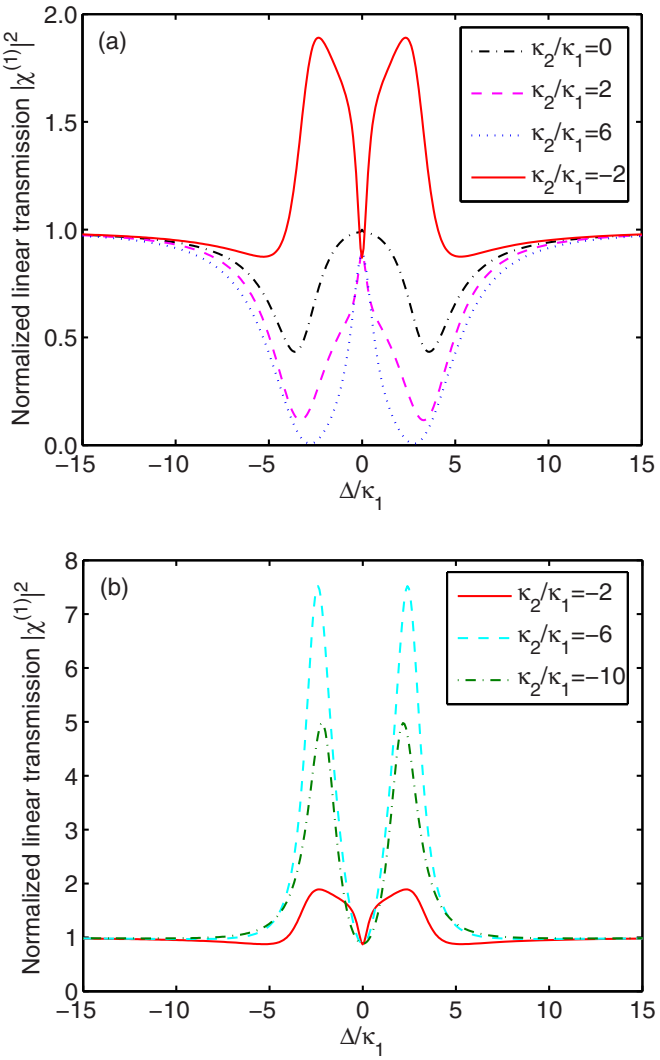

FIG. 3. (Color online) The linear transmission rate $|\chi^{(1)}|^2$ of the probe field as a function of the detuning Δ/κ_1 for several different values of the gain-to-loss ratio, around (a) the transient gain-loss point $\kappa_2/\kappa_1 = 0$ and (b) the balanced gain-loss point $\kappa_2/\kappa_1 = -6$. Note that for the ideal $\mathcal{PT}$-symmetry optics, the necessary condition requires that the gain in the active cavity equals the loss in the passive one (i.e., $\kappa_1 > 0$, $\kappa_e > 0$, $\kappa_2 < 0$, and $\kappa_1 + \kappa_e = -\kappa_2$), which is also called the balanced gain and loss. The other system parameters are chosen as $g_a = 2\kappa_1$, $J = 3\kappa_1$, $\kappa_e = 5\kappa_1$, $\gamma_s = 0.1\kappa_1$, and $\delta = 0$, respectively.

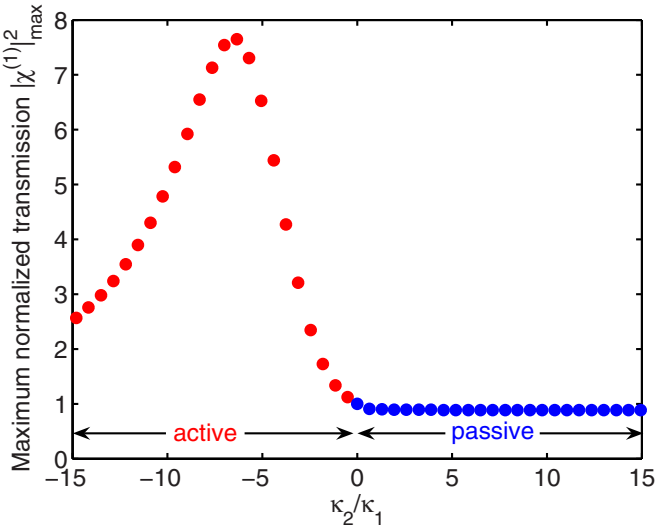

FIG. 4. (Color online) Maximum linear transmission rate $|\chi^{(1)}|^2_{\max}$ of the probe field vs the gain-to-loss ratio κ_2/κ_1. The parameters are the same as in Fig. 3.

According to what has been analyzed in Figs. 2 and 3, we observe that a notable feature of the $\mathcal{PT}$-symmetric double-cavity system is the emerging double-symmetric-sideband peaks of optical amplification when the amount of gain provided to the second cavity supersedes its loss and the cavity becomes an active one. In order to explicitly show the influence of the gain-to-loss ratio on both the DIT and inverted-DIT spectra, in Fig. 4 we display the variation of the transparency on-resonance peak from the passive-passive double cavity and the amplifying double-sideband peaks from the $\mathcal{PT}$-symmetric (i.e., passive-active) double cavity versus the gain-to-loss ratio κ_2/κ_1 in more detail. For a passive-passive double cavity corresponding to $\kappa_2/\kappa_1 > 0$, a single transparency on-resonance peak at $\Delta = 0$ is kept unchanged and is insensitive to the gain-to-loss ratio (see blue solid circle in Fig. 4). For a $\mathcal{PT}$-symmetric double cavity corresponding to $\kappa_2/\kappa_1 < 0$, the two sideband peaks are increased gradually when the gain in the second active cavity is increased, but below the EP. Until the EP, the peaks at both sidebands are maximized. Increasing the gain further leads to the suppression of both of the sideband peaks (see red solid circle in Fig. 4). These results are in good agreement with the above discussions, as shown in Fig. 3.

On the other hand, in Fig. 4 we note that the reduction of the transmission by increasing the gain provides a signature of the $\mathcal{PT}$-broken phase. Thus, it may offer a method to distinguish the $\mathcal{PT}$-symmetric phase and the $\mathcal{PT}$-broken phase via experimentally measuring the optical transmission spectrum.

IV. GREATLY ENHANCED KERR NONLINEARITIES INDUCED BY $\mathcal{PT}$-SYMMETRY BREAKING

In this section, we focus our attention on the nonlinear effects of the $\mathcal{PT}$-symmetric system. Clearly, Eq. (15) is actually a general solution which includes the cases for a passive single cavity, a passive-passive double cavity, and a $\mathcal{PT}$-symmetric (i.e., passive-active) double cavity. There are a large number of parameters that can be adjusted and the corresponding results are given in Figs. 5–9.

Based on an analytical solution for the third-order susceptibility $\chi^{(3)}$ shown in Eq. (15), Fig. 5 presents the Kerr-nonlinear coefficient $\mathrm{Re}[\chi^{(3)}]$ of the physical system as a function of Δ/κ_1 for the three possible configurations: (i) a passive single cavity ($J/\kappa_1 = 0$), (ii) a passive-passive double cavity ($J/\kappa_1 = 3$, $\kappa_2/\kappa_1 = 6$), and (iii) a $\mathcal{PT}$-symmetric (i.e., passive-active) double cavity ($J/\kappa_1 = 3$, $\kappa_2/\kappa_1 = -6$), respectively. It is clearly seen from Fig. 5 that the value of the Kerr-nonlinear coefficient can be dramatically modified by changing the system parameters, e.g., the photon-tunneling strength J and the gain κ_2. Specifically, for an isolated passive cavity

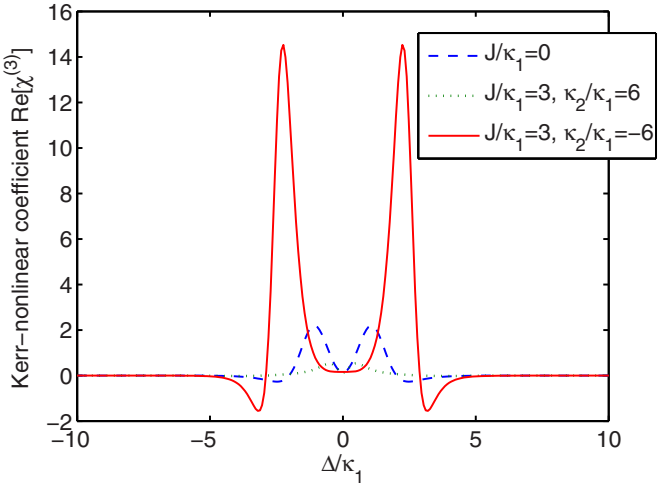

FIG. 5. (Color online) Kerr-nonlinear coefficient $\mathrm{Re}[\chi^{(3)}]$ of the probe field vs the detuning Δ/κ_1 for three different values of the set $(J/\kappa_1, \kappa_2/\kappa_1)$. The other system parameters are the same as in Fig. 2. Here and thereafter, the vertical axis $\mathrm{Re}[\chi^{(3)}]$ is in units of κ_1^{-1}.

$(J/\kappa_1 = 0)$, the Kerr-nonlinear coefficient features a single on-resonance dip between two symmetric sideband peaks. For a passive-passive double cavity $(J/\kappa_1 = 3, \kappa_2/\kappa_1 = 6)$, a single on-resonance dip remains unchanged and two sideband peaks are significantly suppressed. For a $\mathcal{PT}$-symmetric system, a single on-resonance dip still stays the same and two sideband peaks are greatly enhanced. Consequently, the comparison among the three cases can prove an enhanced optical Kerr-nonlinear phenomenon in the $\mathcal{PT}$-symmetric system.

In Fig. 6, we plot the Kerr-nonlinear coefficient $\mathrm{Re}[\chi^{(3)}]$ as a function of Δ/κ_1 for a variety of the gain-to-loss ratio κ_2/κ_1 when J/κ_1 is fixed. Three regimes are clearly identified in Figs. 6(a) and 6(b): (i) non-$\mathcal{PT}$-symmetric regime for $\kappa_2/\kappa_1 > 0$, (ii) unbroken $\mathcal{PT}$-symmetric regime for $-6 < \kappa_2/\kappa_1 < 0$, and (iii) broken $\mathcal{PT}$-symmetric regime for $\kappa_2/\kappa_1 < -6$, respectively. It can be clearly seen that the Kerr-nonlinear coefficient of the probe beam can be dramatically modified by changing the gain-to-loss ratio κ_2/κ_1. The Kerr-nonlinear coefficient is greatly enhanced when one tunes the system parameters so that $\mathcal{PT}$ symmetry is broken, which provides an alternative method to control nonlinear dynamics with a $\mathcal{PT}$-symmetric phase transition. Physically, this is because, in the $\mathcal{PT}$-symmetric phase, the photon-tunneling effects characterized by J are stronger than the intracavity localization effects characterized by $(\kappa_1 + \kappa_e - \kappa_2)/4$. In this case, the weak intracavity field cannot induce enough strong Kerr nonlinearity. On the contrary, in the $\mathcal{PT}$-broken phase, the field localization induces the dynamical accumulations of the optical intensity in the first passive cavity [6,10], corresponding to an increasing third-order Kerr nonlinearity of the system.

In order to further verify the role of the $\mathcal{PT}$-symmetric phase transition, the dependence of the maximum value of the Kerr-nonlinear coefficient $\mathrm{Re}[\chi^{(3)}]_{\max}$ versus the gain κ_2/κ_1 (in units of κ_1) in the second cavity is depicted in Fig. 7. From the red circles in Fig. 7, it is clear that the

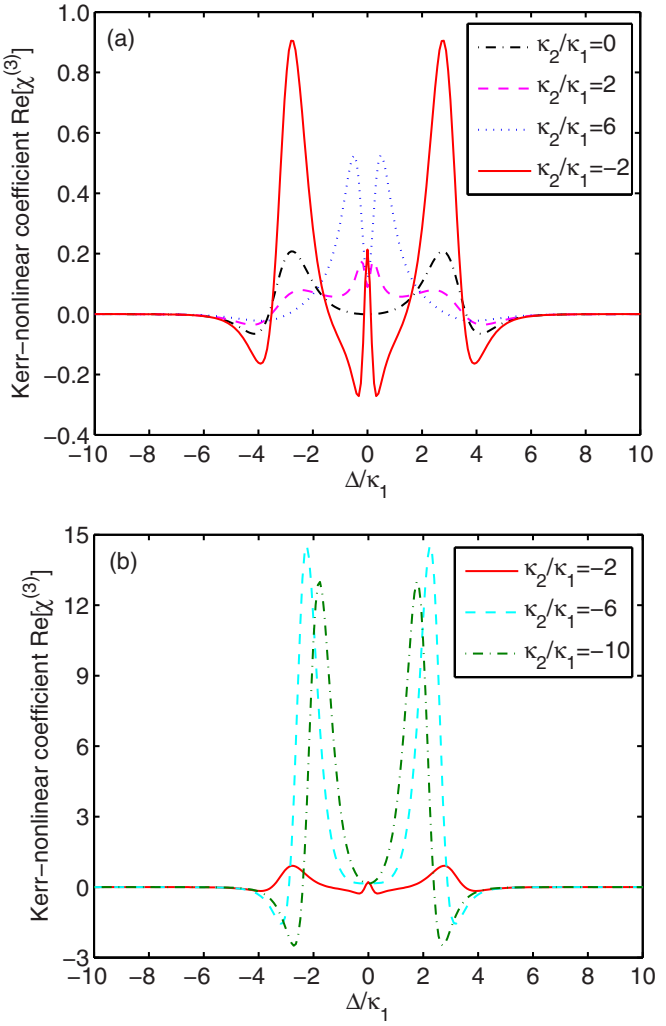

FIG. 6. (Color online) Kerr-nonlinear coefficient $\mathrm{Re}[\chi^{(3)}]$ of the probe field vs the detuning Δ for several different values of the gain-to-loss ratio, around (a) the transient gain-loss point $\kappa_2/\kappa_1 = 0$ and (b) the balanced gain-loss point $\kappa_2/\kappa_1 = -6$. The parameters are the same as in Fig. 3.

maximum values of the Kerr nonlinear coefficient can be dramatically modified at certain probe frequency detunings by changing the gain $\kappa_2/\kappa_1 < 0$ in the second cavity. The maximum value of the Kerr-nonlinear coefficient is increased gradually when the gain is increased until the $\mathcal{PT}$ symmetry is broken. Then, the maximum value of the Kerr-nonlinear coefficient is decreased quickly with further increasing the gain. Note that when $\kappa_2/\kappa_1 > 0$, the $\mathcal{PT}$-symmetric system returns to a passive-passive system shown by the blue circles in Fig. 7.

According to the above analysis, one can conclude that the essence of greatly enhanced Kerr nonlinearities in the $\mathcal{PT}$-broken phase is a dynamical-intensity accumulation induced by optical field localization [6,10]. Because strong intracavity intensity can be accumulated during the $\mathcal{PT}$ transition processes due to the effects of optical field localization, it can induce enough large QE-cavity interactions, which is responsible for giant Kerr nonlinearities.

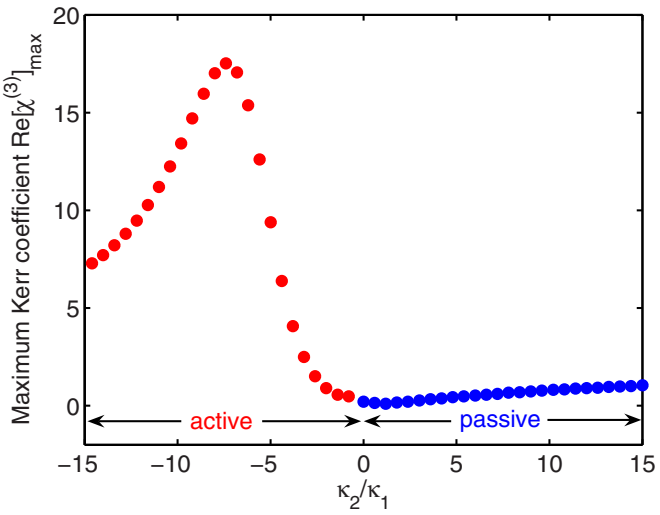

FIG. 7. (Color online) Maximum Kerr-nonlinear coefficient $\mathrm{Re}[\chi^{(3)}]_{\max}$ of the probe field vs the gain-to-loss ratio κ_2/κ_1. The parameters are the same as in Fig. 3.

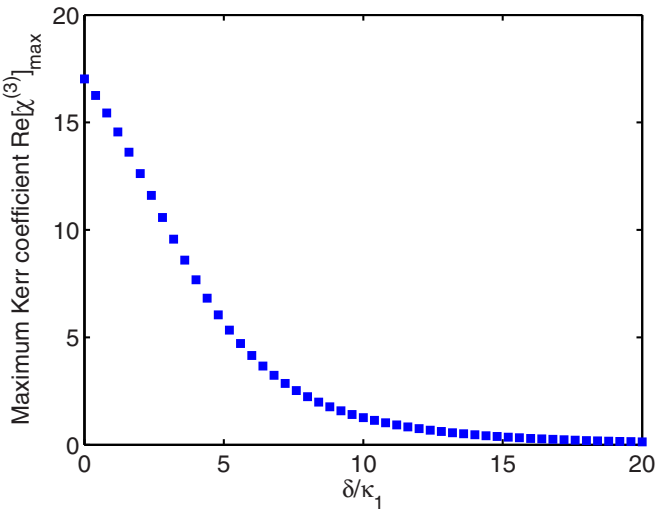

FIG. 9. (Color online) Maximum Kerr-nonlinear coefficient $\mathrm{Re}[\chi^{(3)}]_{\max}$ of the probe field vs the detuning δ/κ_1 for the gain-to-loss ratio $\kappa_2/\kappa_1 = -8$. The other parameters are the same as in Fig. 3.

For the purpose of comparison, in Fig. 8 we simultaneously plot the Kerr-nonlinear coefficient $\mathrm{Re}[\chi^{(3)}]$ (red solid curve), the nonlinear absorption coefficient $\mathrm{Im}[\chi^{(3)}]$ (blue dashed curve), and the linear transmission rate $|\chi^{(1)}|^2$ (green dash-dotted curve) of the weak-probe field as a function of Δ/κ_1 for the balanced gain-to-loss ratio $\kappa_2/\kappa_1 = -6$. From Fig. 8, we find that the maximal Kerr-nonlinear coefficient with vanishing nonlinear absorption and high transmission rate can be obtained with the given practical system parameters. As a specific example, the points a → c → e and b → d → f, standing, respectively, for maximum Kerr-nonlinear coefficient → nonlinear absorption coefficient → linear transmission rate, are clearly shown in Fig. 8. When the maximal Kerr nonlinearity is available in Fig. 8, correspondingly, the nonlinear absorption disappears. At the same time, six times larger than the input probe field can be transmitted in the output waveguide, which are just what we desired. It is well known that a large Kerr-nonlinear coefficient (i.e., index of refraction) with small absorption is useful for dispersion compensation in optical communication [51].

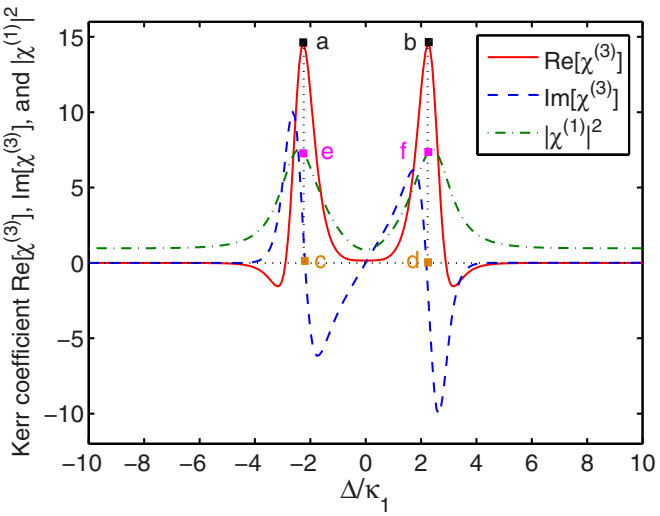

FIG. 8. (Color online) Kerr-nonlinear coefficient $\mathrm{Re}[\chi^{(3)}]$, nonlinear absorption coefficient $\mathrm{Im}[\chi^{(3)}]$, and linear transmission rate $|\chi^{(1)}|^2$ of the probe field as a function of the detuning Δ/κ_1 for the gain-to-loss ratio $\kappa_2/\kappa_1 = -6$. The other parameters are the same as in Fig. 3.

Finally, we turn to illustrate the influences of the detuning δ (the QE's transition frequency ω_e from the cavity resonance frequency ω_0, i.e., $\delta = \omega_e - \omega_0$) and the QE decay rate γ_s on the Kerr-nonlinear coefficient. Figure 9 shows the numerically calculated $\mathrm{Re}[\chi^{(3)}]_{\max}$ as a function of δ/κ_1. We can see that $\mathrm{Re}[\chi^{(3)}]_{\max}$ decreases rapidly with the increase of δ/κ_1. Physically, this is because the QE-cavity-induced interactions become weakened under the change of the detuning δ. In other words, in the existence of δ, the only consequence is that the Kerr-nonlinear effect becomes less efficient. Similar characteristics as in Fig. 9 can be observed with γ_s increasing (not shown here due to the length limitation).

V. CONCLUSIONS

In conclusion, we have provided a detailed mean-field analysis of the steady-state light transmission characteristics and optical Kerr-nonlinear effects as a function of the system parameters in a $\mathcal{PT}$-symmetric structure, composed of a passive loss microcavity and an active gain microcavity. In contrast to the conventional DIT in two passive loss cavities (a single transparency peak arising in the otherwise strong absorptive spectral region), the linear transmission in this $\mathcal{PT}$-symmetric double cavity exhibits an inverted-DIT spectrum, with a nonamplifying transparency dip between two strongly amplifying transmission sideband peaks, providing an analog of the all-optical inverted EIT. Moreover, we find that giant Kerr nonlinearities with high linear transmission rate and vanishing nonlinear absorption can be obtained efficiently when the photon-tunneling-to-loss ratio or the gain-to-loss

ratio is increased to reach a threshold of the symmetry-breaking threshold, that is to say, the $\mathcal{PT}$-symmetry phase transition occurs. The physical mechanism underlying this Kerr-nonlinear enhancement is rooted in the localization-induced dynamical-intensity accumulation [6,10]. The influences of the detuning between the QE and cavity as well as the QE decay rate on optical Kerr nonlinearities are also discussed. The present work opens up avenues for the study of optical nonlinearities observable with low power light. Besides being of interest in itself, optical nonlinearities can find extensive applications in the design of novel optoelectronic $\mathcal{PT}$ devices, such as optical switching, optical memory, logic gates, etc. Conversely, via experimentally measuring the optical transmission spectrum or Kerr-nonlinear coefficient, it also may offer a method to distinguish the $\mathcal{PT}$-symmetric phase and the $\mathcal{PT}$-broken phase.

ACKNOWLEDGMENTS

We appreciate the anonymous referees for their constructive comments to improve the paper. We gratefully acknowledge Dr. Xiaoxue Yang and Xin-You Lü for useful advice and discussion in the manuscript preparation. We also would like to thank Dr. Rong Yu for the enthusiastic help of some numerical simulations. J.L. and Y.W. are supported in part by the National Basic Research Program of China under Contract No. 2012CB922103 and the National Natural Science Foundation of China (NSFC) under Grants No. 11375067 and No. 11574104. X.Z. is supported by the Natural Science Foundation of Hunan Province under Grant No. 14JJ2085 and the PhD Research Startup Foundation of Nanhua University under Grant No. 2013XQD17. C.D. is supported by the NSFC under Grants No. 11447107 and No. U1504111. D.Z. is supported by the NSFC under Grant No. 11404250.

[1] C. M. Bender and S. Boettcher, Phys. Rev. Lett. **80**, 5243 (1998).
[2] C. M. Bender, Contemp. Phys. **46**, 277 (2005).
[3] C. M. Bender, Rep. Prog. Phys. **70**, 947 (2007).
[4] A. Mostafazadeh, J. Math. Phys. **43**, 205 (2002).
[5] A. Guo, G. J. Salamo, D. Duchesne, R. Morandotti, M. Volatier-Ravat, V. Aimez, G. A. Siviloglou, and D. N. Christodoulides, Phys. Rev. Lett. **103**, 093902 (2009).
[6] H. Jing, Ş. K. Ödemir, Z. Geng, J. Zhang, X.-Y. Lü, B. Peng, L. Yang, and F. Nori, Sci. Rep. **5**, 9663 (2015).
[7] A. Regensburger, C. Bersch, M.-A. Miri, G. Onishchukov, D. N. Christodoulides, and U. Peschel, Nature (London) **488**, 167 (2012).
[8] Z. Lin, H. Ramezani, T. Eichelkraut, T. Kottos, H. Cao, and D. N. Christodoulides, Phys. Rev. Lett. **106**, 213901 (2011).
[9] H. Ramezani, T. Kottos, R. El-Ganainy, and D. N. Christodoulides, Phys. Rev. A **82**, 043803 (2010).
[10] B. Peng, Ş. K. Özdemir, F. Lei, F. Monifi, M. Gianfreda, G. L. Long, S. Fan, F. Nori, C. M. Bender, and L. Yang, Nat. Phys. **10**, 394 (2014); also see supplemental material.
[11] L. Chang, X. Jiang, S. Hua, C. Yang, J. Wen, L. Jiang, G. Li, G. Wang, and M. Xiao, Nat. Photon. **8**, 524 (2014).
[12] X. Liu, S. Dutta Gupta, and G. S. Agarwal, Phys. Rev. A **89**, 013824 (2014).
[13] L. Feng, M. Ayache, J. Huang, Y.-L. Xu, M.-H. Lu, Y.-F. Chen, Y. Fainman, and A. Scherer, Science **333**, 729 (2011).
[14] B. Peng, Ş. K. Özdemir, S. Rotter, H. Yilmaz, M. Liertzer, F. Monifi, C. M. Bender, F. Nori, and L. Yang, Science **346**, 328 (2014).
[15] L. Feng, Z. J. Wong, R.-M. Ma, Y. Wang, and X. Zhang, Science **346**, 972 (2014).
[16] H. Hodaei, M.-A. Miri, M. Heinrich, D. N. Christodoulides, and M. Khajavikhan, Science **346**, 975 (2014).
[17] H. Jing, Ş. K. Özdemir, X.-Y. Lü, J. Zhang, L. Yang, and F. Nori, Phys. Rev. Lett. **113**, 053604 (2014).
[18] X.-Y. Lü, H. Jing, J.-Y. Ma, and Y. Wu, Phys. Rev. Lett. **114**, 253601 (2015).
[19] Y. D. Chong, L. Ge, and A. D. Stone, Phys. Rev. Lett. **106**, 093902 (2011).
[20] R. El-Ganainy, K. G. Makris, D. N. Christodoulides, and Z. H. Musslimani, Opt. Lett. **32**, 2632 (2007).
[21] K. G. Makris, R. El-Ganainy, D. N. Christodoulides, and Z. H. Musslimani, Phys. Rev. Lett. **100**, 103904 (2008).
[22] C. E. Rüter, K. G. Makris, R. El-Ganainy, D. N. Christodoulides, M. Segev, and D. Kip, Nat. Phys. **6**, 192 (2010).
[23] N. Bender, S. Factor, J. D. Bodyfelt, H. Ramezani, D. N. Christodoulides, F. M. Ellis, and T. Kottos, Phys. Rev. Lett. **110**, 234101 (2013).
[24] K. J. Vahala, Nature (London) **424**, 839 (2003).
[25] H. J. Kimble, *Cavity Quantum Electrodynamics*, edited by P. Berman (Academic, San Diego, 1994).
[26] H. Mabuchi and A. C. Doherty, Science **298**, 1372 (2002).
[27] J. Vuckovic, arXiv:1402.2541.
[28] H. J. Kimble, Nature (London) **453**, 1023 (2008).
[29] A. Reiserer and G. Rempe, arXiv:1412.2889.
[30] K. Srinivasan and O. Painter, Nature (London) **450**, 862 (2007).
[31] D. Englund, A. Faraon, I. Fushman, N. Stoltz, P. Petroff, and J. Vučković, Nature (London) **450**, 857 (2007).
[32] T. Volz, A. Reinhard, M. Winger, A. Badolato, K. J. Hennessy, E. L. Hu, and A. Imamoglu, Nat. Photon. **6**, 607 (2012).
[33] D. Englund, A. Majumdar, M. Bajcsy, A. Faraon, P. Petroff, and J. Vučković, Phys. Rev. Lett. **108**, 093604 (2012).
[34] R. Bose, D. Sridharan, H. Kim, G. S. Solomon, and E. Waks, Phys. Rev. Lett. **108**, 227402 (2012).
[35] A. Reinhard, T. Volz, M. Winger, A. Badolato, K. J. Hennessy, E. L. Hu, and A. Imamoglu, Nat. Photon. **6**, 93 (2011).
[36] T. G. Tiecke, J. D. Thompson, N. P. de Leon, L. R. Liu, V. Vuletić, and M. D. Lukin, Nature (London) **508**, 241 (2014).
[37] V. Loo, C. Arnold, O. Gazzano, A. Lemaître, I. Sagnes, O. Krebs, P. Voisin, P. Senellart, and L. Lanco, Phys. Rev. Lett. **109**, 166806 (2012).
[38] I. Fushman, D. Englund, A. Faraon, N. Stoltz, P. Petroff, and J. Vučković, Science **320**, 769 (2008).
[39] S. Hughes and C. Roy, Phys. Rev. B **85**, 035315 (2012).
[40] J. Sheng, X. Yang, H. Wu, and M. Xiao, Phys. Rev. A **84**, 053820 (2011).

[41] C. W. Gardiner and P. Zoller, *Quantum Noise* (Springer, Berlin, 2004).
[42] D. F. Walls and G. J. Milburn, *Quantum Optics* (Springer-Verlag, Berlin, 1994).
[43] C. Y. Hu and J. G. Rarity, Phys. Rev. B **91**, 075304 (2015).
[44] A. Majumdar, D. Englund, M. Bajcsy, and J. Vučković, Phys. Rev. A **85**, 033802 (2012).
[45] E. Waks and J. Vuckovic, Phys. Rev. Lett. **96**, 153601 (2006).
[46] E.-M. Graefe, H. J. Korsch, and A. E. Niederle, Phys. Rev. A **82**, 013629 (2010).
[47] S. E. Harris, Phys. Today **50**, 36 (1997).
[48] M. Xiao, Y. Q. Li, S. Z. Jin, and J. Gea-Banacloche, Phys. Rev. Lett. **74**, 666 (1995).
[49] M. Fleischhauer, A. Imamoglu, and J. P. Marangos, Rev. Mod. Phys. **77**, 633 (2005).
[50] Y. Wu and X. X. Yang, Phys. Rev. A **71**, 053806 (2005).
[51] G. P. Agrawal, *Fiber-Optic Communication Systems*, 3rd ed. (Wiley-Interscience, New York, 2002).